Spiral chain models of two-dimensional turbulence

Ö. D. Gürcan,[1] Shaokang Xu,[1,2] and P. Morel[1,3]

[1]*Laboratoire de Physique des Plasmas, CNRS, Ecole Polytechnique, Sorbonne Université, Université Paris-Saclay, Observatoire de Paris, F-91120 Palaiseau, France*

[2]*Peking University, School of Physics, Beijing, China*

[3]*Département de Physique, Université Paris-Sud, Orsay, France*

(Received 25 March 2019; revised manuscript received 20 June 2019; published 25 October 2019)

Reduced models, mirroring self-similar, fractal nature of two-dimensional turbulence, are proposed, using logarithmic spiral chains, which provide a natural generalization of shell models to two dimensions. In a turbulent cascade, where each step can be represented by a rotation and a scaling of the interacting triad, the use of a spiral chain whose nodes can be obtained by scaling and rotating an original wave vector provides an interesting perspective. A family of such spiral chain models depending on the distance of interactions can be obtained by imposing a logarithmic spiral grid with a constant divergence angle and a constant scaling factor and imposing the condition of exact triadic interactions. Scaling factors in such sequences are given by the square roots of known ratios such as the plastic ratio, the super-golden ratio, or some small Pisot numbers. While spiral chains can represent monofractal models of a self-similar cascade, which can span a large range of wave numbers and have good angular coverage, it is also possible that spiral chains or chains of consecutive triads play an important role in the cascade. As numerical models, the spiral chain models based on decimated Fourier coefficients have the usual problems of shell models of two-dimensional turbulence such as the dual cascade being overwhelmed by statistical chain equipartition due to an almost stochastic evolution of the complex phases. A generic spiral chain model based on evolution of energy is proposed, which is shown to recover the dual cascade behavior in two-dimensional turbulence.

DOI: 10.1103/PhysRevE.100.043113

I. INTRODUCTION

Two-dimensional turbulence is a well-studied problem [1–3]. Its basic questions are relatively well understood, and direct numerical simulations with recent computing capabilities provide a reasonable amount of detail for its study [4]. In other words, it is not a physics problem to which one would normally apply "reduction techniques" since direct numerical simulations can already cover a meaningful range of scales. However, there are problems in nature that are rather similar to two-dimensional (2D) turbulence but can be rather demanding in terms of the cost of the description of a large range of scales in these systems. There are many examples, from geophysics [5,6] to plasma physics [7,8], of complex, rich, quasi-two-dimensional problems, which are hard to resolve either due to complexities involving multiscale physics with large-scale separation or complexities of the description itself (for example a 2D kinetic problem requiring four-dimensional simulations [9,10], where reduced models actually become very useful [11,12]). While details such as geometry, boundary conditions, and linear physics in these problems are rather different, advection of (regular or potential) vorticity is a unifying theme [13–15]. Therefore, if a novel reduction scheme is to be proposed for one of these systems, this scheme must first be studied in the setting of 2D turbulence, where the confrontation to physical reality can be achieved more easily due to availability of a relatively good understanding of physical processes and high-resolution direct numerical simulations. In this paper we propose a reduction scheme based on a logarithmic grid in the form of a spiral. This reduction scheme is the natural generalization of shell models [16] to two dimensions, in that while shell models have wave numbers $k_n = k_0 g^n$, spiral chain models have $\mathbf{k}_n = k_0 (g e^{i\alpha})^n$, where g is the scaling factor and α is the divergence angle, in complex vector notation [i.e., $k_{xn}, k_{yn} = \mathrm{Re}(\mathbf{k}_n), \mathrm{Im}(\mathbf{k}_n)$]. In other words, the scaling factor g in the definition of the wave number of the shell model is replaced by the complex number $z = g e^{i\alpha}$. This simple proposition is worth developing since, while multiplication by a real number denotes scaling, multiplication by a complex number denotes "*scaling and rotation.*" Furthermore the systematic "derivation" of these models is proposed by imposing a particular logarithmic spiral grid and keeping only exact triadic interactions, which results automatically in a limited interaction set. Here we introduce these models and demonstrate their use for 2D turbulence and discuss their capabilities and limitations.

Mathematically, the particularity of the spiral form is that it keeps certain quantities (such as the angle between two consecutive elements) invariant as the structure is scaled and rotated. This provides a natural self-similar framework with which some physical systems operate. Spiral patterns emerge in many nonlinear problems in nature, from galaxy formation to crystal growth, from plants to animals, and from atmospheric cyclones to small-scale turbulence, where they appear at very different scales and in very different problems. They are a fundamental element of phyllotaxis, the dynamical phenomenon of arrangement of seeds or petals of a plant (sometimes in the form of flowers) as it grows [17]. One of

the key aspects of phyllotaxis is how a discrete structure that grows through iteration manages *optimal packing*, leading to the observed fractal pattern [18,19]. Similar concepts apply to reaction-diffusion systems where spiral patterns arise in a continuum of deformations [20]. Incidentally, spiral patterns also occur in turbulence [21], especially in two dimensions [6,22], mainly as a result of self-shearing of smaller-scale structures by large-scale flows, and the resulting self-similarity of the turbulent flow, where the structure remains the same as it scales and turns. In fact, the basic motion of scale and rotatation (i.e., "swirl") associated with a turbulent flow naturally implies a spiral-like pattern.

Of course all of these are spirals in real space. However, spirals in wave-vector space are also potentially interesting for the study of turbulent dynamics. Common sense suggests that nonlinear interactions that scale and rotate real space structures would do the same to wave vectors as well. For instance, if we have a particular direction of anisotropy, at a given scale, nonlinearity tends to generate a "next" scale in the hierarchy, which is anisotropic in a direction that is "at a certain angle" to the original direction of anisotropy. Thus, when there is a large-scale source of anisotropy, going towards smaller scales, the direction of anisotropy at each scale keeps changing, which results in a spiral form.

Energy (and enstrophy for two dimensions) gets transferred via triadic interactions in turbulent flows [23,24]. In general for a given scale, there are many such triads that can transfer energy or enstrophy in either direction to other scales. If, for some reason, one of these triads is "dominant," for example, due to the fact that it maximizes the interaction coefficient, it is natural that this triad will take more of the energy or enstrophy along. Then, at the next scale to which the energy goes, the "same triad" (now rotated and scaled), will likely win again for the same reason that it won at the first scale, transferring the energy to the next one along a chain of such dominant triads. It is unclear if the small differences among nearby triads in terms of their capacity to transfer energy and enstrophy justifies a reduction of the turbulent transfer to a picture of *transfer along a single chain of scaled and rotated triads that arrange naturally into a spiral*. Nonetheless the picture of turbulent energy transfer as taking place along chains of spirals that compete with and couple to one another (instead of the naive and incorrect picture of a "radial" flux in k-space) can be thought of as a theoretical picture that can be useful to understand turbulent cascade in Fourier space, whose potential applications to more complex unexplained issues in turbulence remain to be seen.

Various kinds of reduced models have been proposed, in order to study both the nonlinear cascade and the direction of anisotropy in turbulent flows from shell models [16,25], to differential approximation models [26–28], to closure-based models [29,30], to tree models [31–33], to reduced wave-number representations [34] as well as to models based on Galerkin truncation [35,36]. Here we propose a reduction of 2D turbulence based on spiral chains, which are chains of wave numbers that are obtained by scaling and rotating a single triad such that the smaller wave number of the triad, after scaling and rotation (or after a few scalings and rotations), becomes, first, the middle wave number and then the larger wave number. In principle a number of such spiral chains can be used, instead of a single one, in order to span the k-space more completely. Shortcomings of these models should also be mentioned. For example, it is clear that when compared to a regular grid, the logarithmic spiral grid has very little angular resolution in small scales (since the number of resolved angles at a given scale is roughly constant). A more important shortcoming that the basic version of the model shares with shell models of 2D turbulence is that due to randomization of the complex phases, the basic model evolves towards an unphysical chain equipartition solution instead of the inverse energy cascade solution. This is a well-known problem for shell models of 2D turbulence [37], and the usual solution is to increase the number of degrees of freedom as a function of scale using, for example, an hierarchical tree structure [31]. Here we propose an alternative solution which basically gets rid of the phase evolution by considering the evolution of quadratically conserved quantities (in this case energy) directly.

The rest of the paper is organized as follows. In Sec. II the problem of a single triad is revisited, and the concept of triad chains or consecutive triads by which the energy is transferred is discussed. In Sec. III regular spiral chain models for certain chains with relatively local interactions are introduced. The general case of arbitrarily distant interactions is also covered in this section, where a list of possible values of scaling factors and divergence angles is given in Table I. Possible stationary solutions are discussed in Sec. III B, conservation of energy and enstrophy for spiral chains is formulated in Sec. III C, and dual cascade solutions are investigated in Sec. III D. In Sec. IV a spiral chain model formulated for chain energy E_n is introduced. Reinterpreting this model as a model for shell energy, with the assumption of isotropy, which allows the interactions to be infinitesimally local, the continuum limit is computed and found to be the usual differential approximation model form for the two-dimensional Euler turbulence in Sec. IV A. A four-spiral chain model with good angular coverage is introduced in Sec. IV B. Numerical results for a subset of these spiral chain models are given in Sec. V. Section VI is our conclusion.

II. DYNAMICS OF A SINGLE TRIAD

Two-dimensional turbulence, as represented by an equation of advection of vorticity [2], or, more generally, of potential vorticity [38] can be relevant as a simplified limiting case of many physical problems from rotating turbulence in laboratory experiments [39], to geostrophic turbulence in planetary atmospheres [40], to drift wave turbulence in tokamak plasmas [41]. It can be described using a 2D Navier-Stokes equation, written here in terms of the stream function:

$$\partial_t \nabla^2 \Phi + \hat{\mathbf{z}} \times \nabla \Phi \cdot \nabla \nabla^2 \Phi + \mathcal{D}\Phi = 0, \tag{1}$$

where $\mathcal{D}$ could represent viscosity or hyperviscosity necessary for dissipation of energy and enstrophy for the system. Its Fourier transform can be written in general as

$$\partial_t \Phi_k = \sum_{p+q=-k} \frac{\hat{\mathbf{z}} \times \mathbf{p} \cdot \mathbf{q}(q^2 - p^2)}{k^2} \Phi_p^* \Phi_q^* - D_k \Phi_k$$

TABLE I. Table of all spiral chains up to $m = 9$, corresponding to different interaction distances. Note that $\{\ell, m\} = \{2, 3\}$ and $\{\ell, m\} = \{1, 5\}$ have exactly the same g and α and therefore can be combined in a single spiral chain model.

ℓ, m	g	α	s_ℓ	s_m	ℓ, m	g	α	s_ℓ	s_m
1,3	$\sqrt{\psi}$	$\arccos(\frac{g^{-3}}{2})$	+	+	1,8	1.03945070	1.46320427	−	−
2,3	$\sqrt{\rho}$	$\arccos(\frac{g^3}{2})$	−	+		1.06621540	1.25975111	+	+
1,4	1.06333694	1.33527844	−	−		1.08374370	0.84015125	+	−
	1.18375182[†]	0.90934345	+	+	3,8	1.01792429	1.69767863	−	−
3,4	1.18375182[†]	0.53405772	−	+		1.06244389	0.49612812	+	+
1,5	1.09900032	1.73645968	−	+		1.09231550	0.71393754	−	−
	$\sqrt{\rho}$	$\arccos(\frac{g^3}{2})$	+	+		1.10929363	1.21438451	−	+
2,5	1.08646367	0.80694026	+	+	5,8	1.03950336	0.26297678	−	+
	1.16798953	1.16141175	−	−		1.09658675	0.88770503	−	−
3,5	1.05036656	0.42007091	−	+		1.13377435	1.12333647	+	+
	1.18711214	1.38623505	−	−	7,8	1.06295569	0.64055127	+	−
4,5	1.18738019	0.43181263	−	+		1.16615357	0.27659675	−	+
1,6	1.04984644	1.42286906	−	+	1,9	1.02209200	1.29189202	−	−
	1.09917491	1.14794978	+	−		1.04695854	1.66073000	−	+
	1.12611265	0.57438369	+	+		1.06444465	1.11107685	+	+
5,6	1.03282504	0.86317030	+	−		1.07613313	0.74087364	+	−
	1.18224537	0.36320601	−	+	2,9	1.01283840	0.58665015	−	−
1,7	1.01960526	1.20613634	−	+		1.04380602	0.79080898	+	−
	1.06387323	1.45420091	+	+		1.06554885	0.97639366	−	+
	1.09195331	0.97020783	+	−		1.08001175	0.39672051	+	+
	1.10769105	0.48526744	+	+	4,9	1.02868986	0.45935343	+	+
2,7	1.05832758	0.77578744	−	−		1.06421568	1.13693694	−	+
	1.09594733	0.53256457	+	+		1.08867435	1.33411185	+	−
	1.11696283	1.30397985	−	+		1.10276124	0.66651527	−	−
3,7	1.04634171	0.58605974	+	+	5,9	1.01511363	0.23291213	−	+
	1.09867941	1.44528037	−	+		1.05910448	0.94513949	+	+
	1.12854879	0.84668921	−	−		1.09277920	1.67194846	−	+
4,7	1.02518774	0.29962941	−	+		1.11272153	0.73604039	−	−
	1.09707453	1.22673682	+	+	7,9	1.03085468	1.16917138	+	+
	1.14333477	0.96167330	−	−		1.08966388	0.23866415	−	+
5,7	1.08331646	0.30342198	−	+		1.14226818	1.46119977	−	−
	1.16177283	1.43362675	+	+	8,9	1.01340552	0.92556775	−	+
6,7	1.05175240	0.73504742	+	−		1.06962466	0.5679008	+	−
	1.17446465	0.31385868	−	+		1.15808690	0.24742995	−	+

[†]$1.18375182 = \sqrt{1.40126837}$ is the square root of the smallest Salem number of degree 6.

with the convention that $\sum_{p+q=-k}$ represents a sum over $\mathbf{p}$ and $\mathbf{q}$ such that $\mathbf{k} + \mathbf{p} + \mathbf{q} = 0$ (with $p < q$, since the interaction coefficient is symmetrized). Now consider a single triad consisting of $\mathbf{k}$, $\mathbf{p}$, and $\mathbf{q}$ such that $k < p < q$. If $\eta \equiv \frac{\ln(q/k)}{\ln(p/k)} \in \mathbb{Q}$ (i.e., is rational) we can write $p = kg^\ell$ and $q = kg^m$ (i.e., $\eta = m/\ell$). Obviously not all triangles satisfy the condition $\eta \in \mathbb{Q}$. However, there is usually an approximately equivalent triangle from a physics or numerics perspective which does. If one is restricted to low-order rationals for η, it is only a particular class of triangles, which can be represented as $p = kg^\ell$ and $q = kg^m$ with ℓ and m integers and $g > 1$ (i.e., $g \in \mathbb{R}$).

For those triangles, we can write the interaction, without dissipation and forcing as

$$\partial_t \Phi_k = k^2 \sin\alpha_{qp} g^{m+\ell}(g^{2m} - g^{2\ell})\Phi_p^* \Phi_q^*,$$
$$\partial_t \Phi_p = k^2 \sin\alpha_{qp} g^{m-\ell}(1 - g^{2m})\Phi_q^* \Phi_k^*,$$
$$\partial_t \Phi_q = k^2 \sin\alpha_{qp} g^{\ell-m}(g^{2\ell} - 1)\Phi_k^* \Phi_p^*,$$

where we have used $(\hat{\mathbf{z}} \times \hat{\mathbf{p}} \cdot \hat{\mathbf{q}}) = \sin\alpha_{qp} = \sin(\theta_q - \theta_p)$. Since $g > 1$, the middle leg of the triad (i.e., p) is unstable as long as $m > \ell$ (which we have assumed by assuming $q > p$) and gives its energy to the other two wave numbers.

The energy evolves according to

$$\partial_t E_k = (g^{2m} - g^{2\ell})t_{kpq},$$
$$\partial_t E_p = (1 - g^{2m})t_{kpq},$$
$$\partial_t E_q = (g^{2\ell} - 1)t_{kpq},$$

where

$$t_{kpq} = g^{m+\ell} k^4 \sin\alpha_{qp} \Phi_p^* \Phi_q^* \Phi_k^*.$$

It is easy to see that the total energy of the triad is conserved. Following the reasoning discussed in Ref. [42], the instability assumption implies $\overline{t}_{kpq} > 0$ since $\overline{E}_p$ should decrease in time, where the overbar implies the statistical ensemble average, which can be replaced by the time average in most cases.

The energy that is transferred from p to k is $g^{2m} t_{kpq}$, while the energy that is transferred from q to p is simply t_{kpq}. On

the other hand, there is energy that is transferred from k to q (from the smallest to the largest wave number), which is $g^{2\ell}t_{kpq}$. Since $g^{2m} > g^{2\ell}$, E_k gets more energy than it loses. However, since $g^{2\ell} > 1$, E_q also gets more energy than it loses. This means the energy is transferred from the middle wave number to the larger and smaller wave numbers. If the sign of t_{kpq} changes, then the flow will be towards the middle wave number; in fact, the system will naturally undergo such oscillations as the energy of the middle wave number gets depleted.

A. Consecutive triads

Imagine the triad **k**, **p**, **q** discussed above. If we scale it by $g^{-\ell}$ and rotate by $-\theta_p$, we obtain a second triad where **k** becomes the middle wave number instead of the smallest one (we call the other two wave numbers p' and q' with $p' < k < q'$). and if we scale it by g^{-m} and rotate by $-\theta_q$, **k** becomes the largest wave number (with p'' and q'' such that $p'' < q'' < k$). Note that $p' = kg^{-\ell}$, $q' = kg^{m-\ell}$, $p'' = kg^{-m}$, $q'' = kg^{\ell-m}$. By defining $k \to k_n$, and assuming that those three triads exist, we can write the evolution equation for $\Phi_{k_n} \to \Phi_n$, in the absence of forcing and dissipation as

$$\begin{aligned}\partial_t \Phi_n = k_n^2 \sin\alpha_{qp}[&g^{m+\ell}(g^{2m} - g^{2\ell})\Phi^*_{n+\ell}\Phi^*_{n+m} \\ &+ g^{m-3\ell}(1 - g^{2m})\Phi^*_{n-\ell+m}\Phi^*_{n-\ell} \\ &+ g^{\ell-3m}(g^{2\ell} - 1)\Phi^*_{n-m}\Phi^*_{n-m+\ell}]. \end{aligned} \quad (2)$$

The three terms on the right-hand side of (2) are the contributions from (p, q), (p', q'), and (p'', q''), respectively, or to the three triangles from the largest to the smallest. Note that for a given triangle shape, the three terms in (2) appear naturally representing the three different size triangles (but of the same shape), where **k** plays the role of the smallest, the middle, and the largest wave numbers consecutively. In fact, one can also imagine adding a sum over different shapes of triangles in order to provide a complete description.

If we call the triangles from the smallest to the largest $\triangle_1$, $\triangle_2$, and $\triangle_3$, respectively, we obtain $\triangle_2$ by scaling $\triangle_1$ by $g^{m-\ell}$ and rotating it by $\alpha_{qp} = \theta_q - \theta_p$, and $\triangle_3$, by scaling $\triangle_2$ by g^{ℓ} and rotating it by θ_p. Obviously we can repeat the procedure of rotating and scaling in order to cover a whole range of k vectors in the wave-number domain. However, while the scaling is regular (i.e., we can define a $k_n = k_0 g^n$ such that scaled wave numbers always have the form k_n with $n \in \mathbb{Z}$), in general the angles are not perfectly regular.

Consider, for example, the triangle with $g = \sqrt{\varphi}$ where $\varphi = (1 + \sqrt{5})/2$ is the golden ratio so that $k = 1$, $p = g$, and $q = g^2$. The angle between k and p is a right angle (since $\sqrt{1 + g^2} = g^2$ with $g = \sqrt{\varphi}$), while the one between p and q can be computed from the law of cosines as $\cos\alpha_{qp} = \frac{1-p^2-q^2}{2qp} = \frac{1-g^2-g^4}{2g^3}$, which gives an angle about $\alpha_{pq} = 141.83^\circ$ (note that α_{pq} is the angle between the two vectors, which is π minus the angle between the two edges of the triangle). This corresponds to the triangle defined by $\ell = 1$, $m = 2$, and $g = \sqrt{\varphi}$. Scaling this triangle $\triangle_1$ by g and rotating by $\pi/2$, we obtain triangle $\triangle_2$; scaling $\triangle_2$ by g and rotating by 141.83° we obtain $\triangle_3$. We can can construct a chain of such triads that are connected to one another by the common wave number as shown in Fig. 1, for which the equation of motion will still be

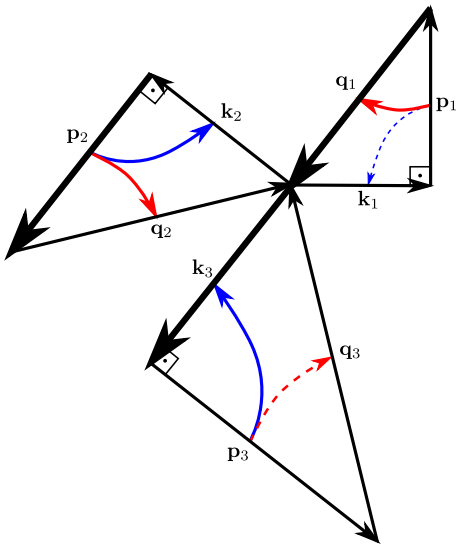

FIG. 1. The triad $\triangle_1$ defined as $\ell = 1$, $m = 2$, $g = \sqrt{\varphi}$. Scaling $\triangle_1$ by g and rotating by $\alpha_{qp} = 141.83^0$, we obtain $\triangle_2$. Scaling $\triangle_2$ by g and rotating by $\pi/2$, we obtain $\triangle_3$. Note that the three triads share the common wave vector $\mathbf{q}_1 = \mathbf{p}_2 = \mathbf{k}_3$, which we can call $\mathbf{k}_n$. The energy inverse cascades via $\mathbf{p}_3 \to \mathbf{k}_n \to \mathbf{k}_2$ (blue arrows, pointing from $\mathbf{p}_i$'s to $\mathbf{k}_i$'s), while enstrophy forward cascades via $\mathbf{p}_1 \to \mathbf{k}_n \to \mathbf{q}_2$ (red arrows, pointing from $\mathbf{p}_i$'s to $\mathbf{q}_i$'s).

(2). However, the grid that is generated by the triad chain is, in general, irregular.

However, it is obvious from this emerging picture that if we had $\alpha_{qp} = m\alpha_{pk}$ where m is some integer, we could write the whole thing as a regular spiral, with $k_n = k_0 g^n$ and $\theta_n = n\alpha$. It is also obvious that the class of triangles that would result in such a regular spiral are a very special class: Each wave number involved in such a system is a rotated and scaled version of the wave number before it in a regular fashion.

III. SPIRAL CHAIN MODELS

A. Particular Chains

Let us introduce the symbol $\mathcal{C}_{\ell m}^{s_\ell s_m}$ to refer to a basic spiral chain consisting of the triad $\mathbf{k}_n + s_\ell \mathbf{k}_{n+\ell} + s_m \mathbf{k}_{n+m} = 0$, where $k_n = k_0 g^n$ and $\theta_n = \alpha n$ [or using the equivalence between 2D vectors and complex numbers, $k_n^c = k_0 (g e^{i\alpha})^n$ with $\mathbf{k}_n = \mathrm{Re}(k_n^c)\hat{\mathbf{x}} + \mathrm{Im}(k_n^c)\hat{\mathbf{y}}$]. Note that g and α follows from ℓ, m, s_ℓ, and s_m and therefore need not be stated explicitly. Here s_ℓ and s_m are the signs in front of the wave numbers in order to satisfy the triad condition.

Considering $\ell = 2$, $m = 3$ in (2), with $\theta_n = n\alpha$, so that $\alpha_{pk} = 2\alpha$, $\alpha_{qp} = \alpha$, and $\alpha_{qk} = 3\alpha$, and all possible interaction forms (i.e., $\mathbf{k} \pm \mathbf{p} \pm \mathbf{q} = 0$), we find that the law of cosines for the different cases gives

$$\cos\alpha_{pk} = \pm\left(\frac{q^2 - k^2 - p^2}{2kp}\right) = \pm\left(\frac{g^6 - g^4 - 1}{2g^2}\right) = \cos 2\alpha,$$

$$\cos\alpha_{qp} = \pm\left(\frac{k^2 - p^2 - q^2}{2pq}\right) = \pm\left(\frac{1 - g^4 - g^6}{2g^5}\right) = \cos\alpha,$$

$$\cos\alpha_{qk} = \pm\left(\frac{p^2 - q^2 - k^2}{2qk}\right) = \pm\left(\frac{g^4 - 1 - g^6}{2g^3}\right) = \cos 3\alpha,$$

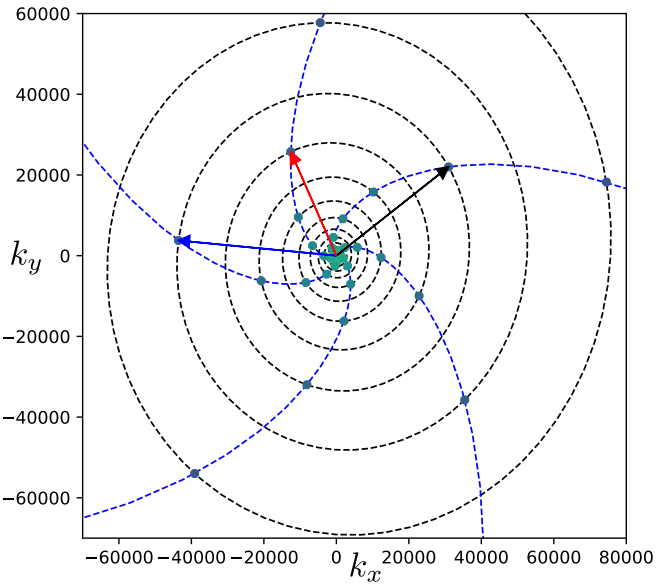

FIG. 2. The spiral chain $\ell = 2$, $m = 3$ with $g = \sqrt{\rho}$. The counterclockwise primary spiral chain is shown by black dashed lines, while the clockwise secondary spirals are shown by blue dashed lines. Note that as the energy travels along the primary chain, it gets exchanged between the five secondary chains. Finally an interacting triad with $\mathbf{k} = \mathbf{k}_n$ (black arrow, pointing right), $\mathbf{p} = \mathbf{k}_{n-2}$ (red arrow, pointing up), and $\mathbf{q} = \mathbf{k}_{n+1}$ (blue arrow, pointing left) is shown (i.e., $\mathbf{k} + \mathbf{q} - \mathbf{p} = 0$).

where the sign $\pm$ corresponds to the relative sign of the two corresponding wave numbers (e.g., p and k for α_{pk}) in the expression $\mathbf{k} \pm \mathbf{p} \pm \mathbf{q} = 0$. We can obtain two polynomial relations for g using the trigonometric relations $\cos 2\alpha = 2\cos^2\alpha - 1$ and $\cos 3\alpha = \cos\alpha(4\cos^2\alpha - 3)$. Both of these can be solved for the cases $\mathbf{k} - \mathbf{p} + \mathbf{q} = 0$ and $\mathbf{k} - \mathbf{p} - \mathbf{q} = 0$ with $g \approx 1.15096$ and an angle $\alpha = \arccos(-g^3/2)$ for the case $\mathbf{k} - \mathbf{p} - \mathbf{q} = 0$ or $\alpha = \pi - \arccos(-g^3/2)$ for the case $\mathbf{k} - \mathbf{p} + \mathbf{q} = 0$. Note that the actual positive root ($g > 1$) of the polynomial equation is $g = \sqrt{\rho}$ where ρ is the plastic number, whose exact value can be written as

$$\rho = \left(\frac{1}{2}\right)^{1/3}\left[\left(1 - \sqrt{\frac{23}{27}}\right)^{1/3} + \left(1 + \sqrt{\frac{23}{27}}\right)^{1/3}\right].$$

1. Chain $\mathcal{C}^{-,-}_{2,3}$

The basic chain, shown in Fig. 2 can be denoted by $C^{-,-}_{2,3}$, for which an evolution equation can be written as

$$\begin{aligned}\partial_t \Phi_n = k_n^2 \sin\alpha[&g^{-7}(g^4 - 1)\Phi_{n-3}\Phi^*_{n-1} \\ &- g^{-3}(g^6 - 1)\Phi_{n-2}\Phi^*_{n+1} \\ &+ g^9(g^2 - 1)\Phi_{n+2}\Phi_{n+3}] + P_n - D_n\Phi_n \end{aligned} \quad (3)$$

with $\Phi_n = \hat{\Phi}(\mathbf{k}_n)$ as the Fourier coefficient of Φ, with the wave vector $\mathbf{k}_n = k_n(\cos\alpha_n, \sin\alpha_n)$, where $k_n = k_0 g^n$ and $\alpha_n = \alpha n$, $g = \sqrt{\rho}$ being the logarithmic scaling factor and $\alpha = \arccos(-g^3/2)$ being the divergence angle. P_n and D_n are injection and dissipation, respectively (i.e., $D_n = \nu k_n^2$ for a usual kinematic viscosity and $P_n = \gamma_n \Phi_n$ for an internal instability drive).

Note that using the relations $g^6 - 1 = g^2$, $g^4 - 1 = g^{-2}$, and $g^2 - 1 = g^{-8}$, possible due to the choice $g = \sqrt{\rho}$, we can write (3) also as

$$\begin{aligned}\partial_t \Phi_n = k_n^2 \sin\alpha[&g^{-9}\Phi_{n-3}\Phi^*_{n-1} - g^{-1}\Phi_{n-2}\Phi^*_{n+1} \\ &+ g\Phi_{n+2}\Phi_{n+3}] + P_n - D_n\Phi_n. \end{aligned} \quad (4)$$

While (4) conserves energy and enstrophy for $g = \sqrt{\rho}$, (3) does so for arbitrary g, which makes it somewhat more useful even though the two equations are identical for the given value of g.

2. Chain $\mathcal{C}^{-,+}_{2,3}$

It is clear that there are many similar chains, such as the one with $\alpha = \pi - \arccos(-g^3/2) = \arccos(g^3/2)$, which gives a similar model but with a different conjugation structure:

$$\begin{aligned}\partial_t \Phi_n = k_n^2 \sin\alpha[&g^{-7}(g^4 - 1)\Phi^*_{n-3}\Phi_{n-1} - g^{-3}(g^6 - 1)\Phi_{n+1}\Phi_{n-2} \\ &+ g^5(g^6 - g^4)\Phi_{n+2}\Phi^*_{n+3}] + P_n - D_n\Phi_n \end{aligned} \quad (5)$$

and a different sampling of wave-vector directions.

3. Chain $\mathcal{C}^{+,+}_{-1,2}$ (or $\mathcal{C}^{+,+}_{1,3}$)

We can obtain another chain by choosing $\ell = -1$, $m = 2$, which gives $\alpha_{pk} = -\alpha$, $\alpha_{qp} = 3\alpha$, and $\alpha_{qk} = 2\alpha$. Using the law of cosines and the relations between $\cos\alpha$, $\cos 2\alpha$, and $\cos 3\alpha$, we obtain $g \approx 1.21061$, or $g = \sqrt{\psi}$ where

$$\psi = \frac{1}{3}\left\{1 + \frac{1}{2^{1/3}}[(29 + 3\sqrt{93})^{1/3} + (29 - 3\sqrt{93})^{1/3}]\right\}$$

is the so-called super-golden ratio, and $\alpha = \arccos(g^{-3}/2)$ for the form $\mathbf{k} + \mathbf{p} + \mathbf{q} = 0$, and thus an evolution equation of the form

$$\begin{aligned}\partial_t \Phi_n = k_n^2 \sin\alpha[&g^{-11}(g^2 - 1)\Phi^*_{n-2}\Phi^*_{n-3} \\ &- g^{-3}(g^6 - 1)\Phi^*_{n-1}\Phi^*_{n+2} + g^3(g^4 - 1)\Phi^*_{n+3}\Phi^*_{n+1}] \\ &+ P_n - D_n\Phi_n, \end{aligned} \quad (6)$$

where we have used the fact that for this particular value of α, we have $\sin 3\alpha = -g^{-2}\sin\alpha$.

4. Chain $\mathcal{C}^{-,+}_{-1,2}$ (or $\mathcal{C}^{-,-}_{1,3}$)

A similar case to chain $\mathcal{C}^{+,+}_{-1,2}$ exists with $g = \sqrt{\psi}$ and $\alpha = \arccos(-g^{-3}/2) = \pi - \arccos(g^{-3}/2)$, which corresponds to $\mathbf{k} + \mathbf{q} - \mathbf{p} = 0$ and the evolution equation of the form

$$\begin{aligned}\partial_t \Phi_n = k_n^2 \sin\alpha[&g^{-11}(g^2 - 1)\Phi^*_{n-2}\Phi_{n-3} \\ &- g^{-3}(g^6 - 1)\Phi_{n-1}\Phi^*_{n+2} + g^3(g^4 - 1)\Phi_{n+3}\Phi_{n+1}] \\ &+ P_n - D_n\Phi_n. \end{aligned}$$

The chain denoted by $\ell = 1$, $m = 3$ corresponds to the same chain as the one denoted by $\ell = -1$, $m = 2$ (since we can obtain one from the other by exchanging k and p). This means we can write $\mathcal{C}^{+,+}_{-1,2} = \mathcal{C}^{+,+}_{1,3}$ and $\mathcal{C}^{-,+}_{-1,2} = \mathcal{C}^{-,-}_{1,3}$ or in general $\mathcal{C}^{s_\ell, s_m}_{\ell,m} = \mathcal{C}^{s_\ell, s_m * s_\ell}_{-\ell, m-\ell}$. This means that it is sufficient to consider the case $m > \ell > 0$.

5. Chains $\mathcal{C}^{-,-}_{2,3} + \mathcal{C}^{-,-}_{1,5}$

Remarkably, the case $\ell = 1$ and $m = 5$ gives $g = \sqrt{\rho}$ and $\alpha = \arccos(-g^3/2)$ exactly as in the case $\ell = 2$ and $m = 3$. This means that in fact these two spiral chains are inseparable since a choice of g and α will lead to an evolution equation of the form

$$\begin{aligned}\partial_t \Phi_n = k_n^2 \sin\alpha[&-g^{-19}(g^2-1)\Phi_{n-5}\Phi^*_{n-4}\\ &+ g^{-7}(g^4-1)\Phi_{n-3}\Phi^*_{n-1} - g^{-3}(g^6-1)\Phi_{n-2}\Phi^*_{n+1}\\ &+ g^{-3}(g^{10}-1)\Phi_{n-1}\Phi^*_{n+4} - g^{3}(g^8-1)\Phi_{n+1}\Phi_{n+5}\\ &+ g^{9}(g^2-1)\Phi_{n+2}\Phi_{n+3}] + P_n - D_n\Phi_n. \end{aligned} \tag{7}$$

It is easy to show that these are in fact *all the interactions* that take place among the points of this particular spiral (i.e., defined by g and α). Similarly there is another double chain of the form $\mathcal{C}^{-,+}_{2,3} + \mathcal{C}^{+,+}_{1,5}$ as well.

6. Supplementary chains

Consider the two chains represented by $\mathcal{C}^{+,+}_{1,3}$ and $\mathcal{C}^{-,-}_{1,3}$ discussed above. The two chains have the same g's but supplementary angles. This means that while the $++$ chain has the angles $\theta_n = n\alpha$, the supplementary chain has the angles $\theta_n = n(\pi - \alpha)$. However, since both Φ_n and Φ^*_n are considered for a given $\mathbf{k}_n$, adding or subtracting π to an angle is equivalent to taking the complex conjugate or replacing $\mathbf{k}_n \to -\mathbf{k}_n$. Therefore we can instead use $\theta_n = -n\alpha$, and note that it corresponds to the spiral that rotates in the opposite direction to the original spiral, but with $\mathbf{k}_n + \mathbf{k}_{n+1} + \mathbf{k}_{n+3} = 0$, since the signs of $k_{n\pm\ell}$ for odd ℓ change direction.

7. Other chains

If we consider other ℓ and m values, it is clear that $\ell = 4$, $m = 6$ gives $g_{4,6} = (g_{2,3})^{1/2}$ and $\alpha_{4,6} = \alpha_{2,3}/2$, etc. These are not unique chains but simply the same chains that are repeated twice [or n times to get $g_{2n,3n} = (g_{2,3})^{1/n}$, and $\alpha_{2n,3n} = \alpha_{2,3}/n$]. In contrast, for a unique chain, we have to compute g and α. In general, for any ℓ and m such that $\mathbf{k}_n + s_\ell \mathbf{k}_{n+\ell} + s_m \mathbf{k}_{n+m} = 0$, we can write

$$\begin{aligned}\cos\ell\alpha &= s_\ell \frac{(g^{2m} - g^{2\ell} - 1)}{2g^\ell},\\ \cos m\alpha &= s_m \frac{(g^{2\ell} - g^{2m} - 1)}{2g^m},\\ \cos(m-\ell)\alpha &= s_m s_\ell \frac{(1 - g^{2m} - g^{2\ell})}{2g^{(m+\ell)}}.\end{aligned}$$

Consistency requires that

$$\begin{aligned}&\frac{1}{\ell}\arccos\left[s_\ell \frac{(g^{2m} - g^{2\ell} - 1)}{2g^\ell}\right]\\ &\quad= \frac{1}{m}\arccos\left[s_m \frac{(g^{2\ell} - g^{2m} - 1)}{2g^m}\right]\\ &\quad= \frac{1}{m-\ell}\arccos\left[s_\ell s_m \frac{(1 - g^{2m} - g^{2\ell})}{2g^{(m+\ell)}}\right],\end{aligned} \tag{8}$$

where the arccos function is considered as multivalued. These equations can be solved numerically in order to obtain spiral chains for any ℓ and m values. In general for a given ℓ and m, one may have multiple solutions of (8) because of the multivaluedness of the arccosine functions. Note that the combination of s_ℓ and s_m and g defines a unique angle α. See Table I for a list of all possible chains up to $m = 9$. Note that for each chain that is represented in Table I, there is also the supplementary chain with $\alpha' = \pi - \alpha$ and $s'_\ell = \begin{cases} s_\ell & \ell\text{: even} \\ -s_\ell & \ell\text{: odd} \end{cases}$ and $s'_m = \begin{cases} s_m & m\text{: even} \\ -s_m & m\text{: odd} \end{cases}$.

B. Power-law steady-state solutions

Substituting $\Phi_n \to A k_n^\alpha$ in (2), the nonlinear term vanishes when

$$\begin{aligned}&g^{(\alpha+3)m+(\alpha+1)\ell} - g^{m(\alpha+1)+(\alpha+3)\ell}\\ &\quad+ g^{(\alpha+1)m-(2\alpha+3)\ell} - g^{(\alpha+3)m-(2\alpha+3)\ell}\\ &\quad+ g^{(\alpha+3)\ell-(2\alpha+3)m} - g^{(\alpha+1)\ell-(2\alpha+3)m} = 0,\end{aligned}$$

which can be satisfied if (a) $(\alpha+1) = -(2\alpha+3)$ (i.e., $\alpha = -4/3$) independent of the value of ℓ and m, in which case the first term cancels the fourth one, the second term cancels the fifth, and the third term cancels the last one, or (b) $(\alpha+3) = -(2\alpha+3)$ (i.e., $\alpha = -2$), where the first term cancels the last one, the second term cancels the third one, and the fourth term cancels the fifth one. These correspond to the usual Kraichnan-Kolmogorov spectra $E(k) \propto \{k^{-3}, k^{-5/3}\}$ since $E(k_n) \equiv \Phi_n^2 k_n$ [3]. Note that these self-similar power-law solutions on any spiral chain $\mathcal{C}^{s_\ell,s_m}_{\ell,m}$ may be anisotropic in the sense that $\Phi_{k_x,0} \neq \Phi_{0,k_y}$ for a given scale are isotropic in the sense that if we average over a few consecutive scales we get a solution that is independent of the direction of k. The details of the relation of these solutions to the dual cascade are further discussed in Sec. III D.

However, numerical integration of the model with energy injected roughly in the middle of the spiral does not seem to converge to these solutions (see Sec. V). Instead it seems that the Φ_n act as "random" variables, and the system goes to a chain equipartition solution expected from statistical equilibrium such that $P(\Phi_n) = e^{-(\beta_1 k_n^4 |\Phi_n|^2 + \beta_2 k_n^2 |\Phi_n|^2)/2}$, which gives (i.e., $T_1 = \beta_1^{-1}$ and $T_2 = \beta_2^{-1}$)

$$\langle|\Phi_n|^2\rangle = \frac{T_1}{k_n^4 + \frac{T_1}{T_2}k_n^2}$$

and thus a spectral energy density scaling of the form $E(k) \propto \{k^{-3}, k^{-1}\}$. In general, which of these solutions will be observed depends on various factors from numerical details to the way the system is driven. In practice, the chain equipartition does not give a clean k^{-1} spectrum either (e.g., see Sec. V). It is likely that the resulting spectrum is actually that of an equipartition along a structure of fractal dimension [43] implied by the spiral chain. which could be thought of as a Fourier space decimation [44].

C. Energy and enstrophy

Multiplying (2) by $\Phi_n^* k_n^2$ and taking the real part, we can write the evolution of energy:

$$\partial_t E_n = \left[(g^{2m} - g^{2\ell}) t^E_{n+\ell} + (1 - g^{2m}) t^E_n + (g^{2\ell} - 1) t^E_{n-m+\ell}\right] + P^E_n - D^E_n, \tag{9}$$

where $E_n = k_n^2 |\Phi_n|^2$

$$t^E_n \equiv \mathrm{Re}\left[g^{m-3\ell} k_n^4 \sin\alpha_{qp} \Phi^*_{n-\ell+m} \Phi^*_{n-\ell} \Phi^*_n\right], \tag{10}$$

or multiplying (2) by $\Phi_n^* k_n^4$,

$$\partial_t W_n = \left[(g^{2(m-\ell)} - 1) t^W_{n+\ell} + (1 - g^{2m}) t^W_n + (g^{2m} - g^{2(m-\ell)}) t^W_{n-m+\ell}\right] + P^W_n - D^W_n, \tag{11}$$

where $W_n = k_n^4 |\Phi_n|^2$, and

$$t^W_n \equiv \mathrm{Re}\left[g^{m-3\ell} k_n^6 \sin\alpha_{qp} \Phi^*_{n-\ell+m} \Phi^*_{n-\ell} \Phi^*_n\right]. \tag{12}$$

It is easy to see that total energy $E = \sum_n E_n$ and total enstrophy $W = \sum_n W_n$ are conserved since t_n's cancel each other at different orders. This is basically due to the fact that each triad conserves energy and enstrophy, and thus each chain of triads represented by the spiral chain conserves energy and enstrophy independently. Consider a midscale, well-localized drive (say, around the wave number k_f), with both large-scale and small-scale dissipations. If we sum over (9) from $n = 0$ up to an n such that $k_n < k_f$, in the inertial range for energy, we get

$$\partial_t \sum_{n'=0}^{n} E_{n'} + \Pi^E_n = -\varepsilon_\ell,$$

where ε_ℓ is the total large-scale energy dissipation and

$$\Pi^E_n \equiv -\left[(g^{2m} - g^{2\ell}) \sum_{j=1}^{m} t^E_{n-m+\ell+j} + (1 - g^{2m}) \sum_{j=1}^{m-\ell} t^E_{n-m+\ell+j}\right]. \tag{13}$$

A statistical steady state may imply

$$\overline{\Pi}^E_n = -\varepsilon_\ell, \tag{14}$$

and if $\bar{t}^E_n$ is independent of n for an inertial range, we can write

$$\overline{\Pi}^E_n = -\lambda_E \bar{t}^E_n, \tag{15}$$

where $\lambda_E = [(1 - g^{2\ell})m - (1 - g^{2m})\ell]$. Note that for $g = 1 + \epsilon$, so that $g^{2\ell} = 1 + 2\ell\epsilon + (2\ell^2 - \ell)\epsilon^2$ and finally $\lambda = 2(m - \ell)m\ell\epsilon^2 > 0$, since $m > \ell$. If we increase g, $\lambda > 0$ will be more easily satisfied. So practically for any $g > 1$ and $\ell > m$, we have $\lambda > 1$.

Note that the instability assumption of a single triad discussed in Sec. II for an arbitrary triad implies $\bar{t}^E_n > 0$, resulting in an inverse cascade of energy (i.e., $\overline{\Pi}^E_n < 0$). Similarly by computing the sum over (11) from n to N such that $k_n > k_f$ is in the inertial range for enstrophy,

$$\partial_t \sum_{n'=n}^{N} W_{n'} - \Pi^W_n = -\varepsilon_s,$$

where ε_s is the total small-scale dissipation and

$$\Pi^W_n \equiv \left[(g^{2(m-\ell)} - 1) \sum_{j=1}^{m} t^W_{n-m+\ell+j} + (1 - g^{2m}) \sum_{j=1}^{m-\ell} t^W_{n-m+\ell+j}\right] \tag{16}$$

is the k-space flux of enstrophy. A statistical steady state would imply

$$\overline{\Pi}^W_n = \varepsilon_s, \tag{17}$$

and therefore a constant $\bar{t}^W_n$ that is independent of n. This gives

$$\overline{\Pi}^W_n = \lambda_W \bar{t}^W_n, \tag{18}$$

where

$$\lambda_W \equiv (1 - g^{2m})(m - \ell) - (1 - g^{2(m-\ell)})m > 0,$$

which can be seen from the fact that λ_W has the same form as λ_E but ℓ replaced by $m - \ell$ and $m - \ell < m$. The instability assumption for a single triad suggests $\bar{t}^W_n > 0$, so we get a forward cascade of enstrophy.

D. Dual cascade solutions

In addition of the direction of the cascade, the above formulation can be used to obtain the cascade solutions. Recall that the idealized picture of the dual cascade is that of a forward cascade of enstrophy consisting of a constant enstrophy flux accompanied by zero energy flux and an inverse cascade of energy consisting of a constant (negative) flux of energy accompanied by zero enstrophy flux. In real turbulence, these solutions are manifested statistically, while in a reduced model they may appear as exact solutions of the model.

Let us consider the solution for the forward enstrophy cascade range. In this case we would have $\overline{\Pi}^E_n = 0$ and $\overline{\Pi}^W_n = \varepsilon_s$ as in (17), and this gives $\bar{t}^W_n = \varepsilon_s/\lambda_W$ a constant independent of n [see Eq. (18)]. When this solution is substituted into $\bar{t}^E_n = \bar{t}^W_n k_n^{-2} = \varepsilon_s k_n^{-2}/\lambda_W$, we find from (13) that

$$\overline{\Pi}^E_n = -\frac{\varepsilon_s}{\lambda_W k^2_{n-m+\ell+1}} \left[(g^{2m} - g^{2\ell}) \sum_{j=0}^{m-1} g^{-2j} + (1 - g^{2m}) \sum_{j=0}^{m-\ell-1} g^{-2j}\right],$$

and using the relation $\sum_{j=0}^{m-1} g^{-2j} = \frac{(1-g^{-2m})}{(1-g^{-2})}$, it is easy to see that

$$\overline{\Pi}^E_n = -\frac{\varepsilon_s k^{-2}_{n-m+\ell+1}}{\lambda_W (1 - g^{-2})} [(g^{2m} - g^{2\ell})(1 - g^{-2m}) + (1 - g^{2m})(1 - g^{-2(m-\ell)})] = 0.$$

Using the definition t^W_n from (12), assuming Φ_n is a power law, or using $\bar{t}^E_n \sim k_n^{-2}$, and $\bar{t}^E_n \propto k_n^4 \langle |\Phi_n|^3 \rangle$, one obtains a spectral energy density of the form $E(k_n) = |\Phi_n|^2 k_n \propto k_n^{-3}$ for the forward enstrophy cascade range. This solution satisfies both $\overline{\Pi}^W_n = \varepsilon_s$ and $\overline{\Pi}^E_n = 0$ simultaneously as it should.

Similarly for the inverse energy cascade range, we have a constant energy flux $\overline{\Pi}^E_n = -\mathcal{E}_\ell$ as in (14), and zero enstrophy

flux, $\overline{\Pi}_n^W = 0$. These conditions give $\bar{t}_n^E = \mathcal{E}_\ell/\lambda_E$, which is a constant independent of n [see Eq. (15)] and $\bar{t}_n^W = \mathcal{E}_\ell k_n^2/\lambda_E$. Substituting this into the definition of $\overline{\Pi}_n^W$ from (16), we find that it satisfies the condition that $\overline{\Pi}_n^W = 0$.

Note finally that the requirement, for example, that $\bar{t}_n^W$ be a constant means

$$\bar{t}_n^W = g^{m-3\ell} k_n^6 \sin\alpha_{qp} \Phi_{n-\ell+m} \Phi_{n-\ell} \Phi_n \times \langle \cos(\phi_{n-\ell+m} + \phi_{n-\ell} + \phi_n) \rangle.$$

Now, if the phases ϕ_n become random, the average of a cosine of the sum of these random variables would be very small and would not allow much transfer. Since there are no other triads through which the enstrophy can flow to small scales in such a model, the cascade may be overwhelmed by the statistical equipartition solution that we discussed at the end of Sec. III B. One way to fix this issue for numerical convenience is to get rid of this detailed phase evolution as we will discuss in the following section.

IV. THE MODEL FOR E_n

The general model for the evolution of turbulent energy on the spiral chain can be formulated as

$$\partial_t E_n = \left[(g^{2m} - g^{2\ell}) t_{n+\ell}^E + (1 - g^{2m}) t_n^E + (g^{2\ell} - 1) t_{n-m+\ell}^E\right] + P_n^E - D_n^E, \tag{19}$$

where

$$t_n^E = g^{-\ell} k_n \sin[(m-\ell)\alpha] E_n^{3/2}. \tag{20}$$

Note that $E(k_n) = E_n k_n^{-1}$ and that $E_n > 0$ and $P_n^E > 0$ to ensure realizability. The model still conserves energy and enstrophy and results in a clean dual cascade solution. And the difference from a model that solves the complex amplitudes Φ_n is mainly in the definition (10) versus (20). The two models would become "equivalent" if the sums of the complex phases would vanish at each scale (for example, for $\ell = 2$, $m = 3$, this would mean $\phi_n + \phi_{n+1} - \phi_{n-2} = 0$, where ϕ_n are the complex phases). The condition is nontrivial and is not satisfied in the nonlinear stage by a complex chain model for Φ_n. Hence the complex chain fails to describe the cascade but instead evolves towards statistical chain equipartition.

The model in (19) works for any ℓ and m combination given in Table I, but one should pay attention to the fact that as ℓ and m change, g and therefore the range of wave numbers that are covered by the model change, which means that the dissipation and the boundary terms should also be modified accordingly. Note finally that the assumption of $t_n^E \propto k_n E_n^{3/2}$ is in fact similar to Kovasznay's hypothesis for the transfer function as discussed in Monin and Yaglom [45].

A. Continuum limit

It is also possible to interpret (19) as a shell model by disregarding the information on angles and therefore lifting the restriction on g values. In this case the resulting model is a simple discrete formulation of a general model where any value of g is allowed and an arbitrary factor [instead of the $\sin(m-\ell)\alpha$] multiplies the nonlinear term, as in shell models. This interpretation allows us to transform the problem into a differential approximation model by considering the continuum limit of (19), with $\ell = 1$, $m = 2$, by considering $g \to 1 + \epsilon$. Define $E(k) = E_n k_n^{-1}$ and $F(k) = k^{3/2} E(k)^{3/2}$, so that $k_{n+1} = k(1+\epsilon)$ and $k_{n-1} = k(1 - \epsilon + \epsilon^2)$ so that

$$F(k_{n+1}) \approx \left(F + k\epsilon \frac{dF}{dk} + \frac{1}{2}\epsilon^2 k^2 \frac{d^2F}{dk^2}\right),$$

$$F(k_{n-1}) \approx \left[F(k) - k(\epsilon - \epsilon^2)\frac{dF}{dk} + \frac{1}{2}\epsilon^2 k^2 \frac{d^2F}{dk^2}\right],$$

and

$$\left[g^2 k_n^{-1} t_{n+1}^E - (1+g^2) k_n^{-1} t_n^E + k_n^{-1} t_{n-1}^E\right] \approx 3\epsilon^2 F + 5\epsilon^2 k \frac{dF}{dk} + \epsilon^2 k^2 \frac{d^2F}{dk^2}.$$

This finally gives

$$\partial_t E - C \frac{\partial}{\partial k}\left[k^{-1} \frac{\partial}{\partial k}\left(k^{9/2} E^{3/2}\right)\right] = P_E(k) - D_E(k) \tag{21}$$

as a differential approximation model [26]. It is clear that the two solutions $E(k) \propto k^{-5/3}$ and $E(k) \propto k^{-3}$ both cause the nonlinear term to vanish. In fact, the way that the flux is approximated, it works nicely that $k^{-5/3}$ gives a constant and negative energy flux. In fact, the constant flux solution of the above equation is $E(k) = (\frac{\varepsilon_\ell}{2C})^{2/3} k^{-5/3}$, which is helpful for picking the value of C in order to normalize the model properly. The continuum limit as discussed above results in an isotropic model, since its derivation starts from a shell model with no regard to angles.

B. Four-spiral chain model

Considering the model in (7) and using four such spiral chains that are basically rotated by $\delta\alpha = j\alpha/4$ and scaled by $g^{j/4}$ where $j = 1, 2, 3$ with respect to the original spiral (together with the original spiral itself; see Fig. 3) gives us a four-spiral chain model, where the each spiral chain is coupled with itself but not with the other three. The advantage of the existence of the other chains is therefore a better coverage of the k-space but not a better description of the nonlinear interaction (i.e., the number of triads in the four-spiral chain model is basically four times the single-spiral chain one). Such a model can be formulated alternatively by defining $g = \rho^{1/8}$ and $\alpha = \frac{1}{4}\arccos(-\frac{g^{12}}{2})$ and using $\mathbf{k_n} = \boldsymbol{k_n}(\cos\boldsymbol{\alpha_n}, \sin\boldsymbol{\alpha_n})$, where $k_n = k_0 g^n$ and $\alpha_n = \alpha n$ as usual (note that g here is obviously different from the earlier one). The evolution for Φ can then be written as

$$\partial_t E_n = k_n \sin\alpha \left[g^{16}(g^8 - 1) E_{n+8}^{3/2} + (g^{32} - 1) g^{-12} E_{n+4}^{3/2} + [g^{-8} - 2g^{16} + g^{-24}] E_n^{3/2} + (g^{16} - 1) g^{-12} E_{n-4}^{3/2} + (g^8 - 1) g^{-40} E_{n-16}^{3/2}\right] + P_n^E - D_n^E. \tag{22}$$

Please note the simplicity of the nonlinear couplings in this model. Albeit the fact that the model considers two kinds of triangles and spans roughly about 10 different directions for a given "scale" it represents these nonlinear interactions with only five terms.

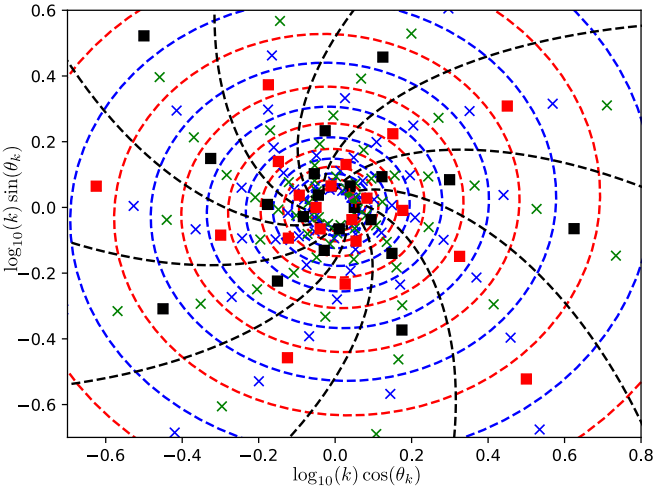

FIG. 3. The four-spiral chain grid shown explicitly. The original spiral chain is shown by black squares, while its reflection with respect to the origin is shown by red squares (if in color). The full system is symmetric with respect to reflection $\mathbf{k} \to -\mathbf{k}$, and therefore one can actually use only half of the k-plane (e.g., the upper half) and obtain the rest of the points by reflection.

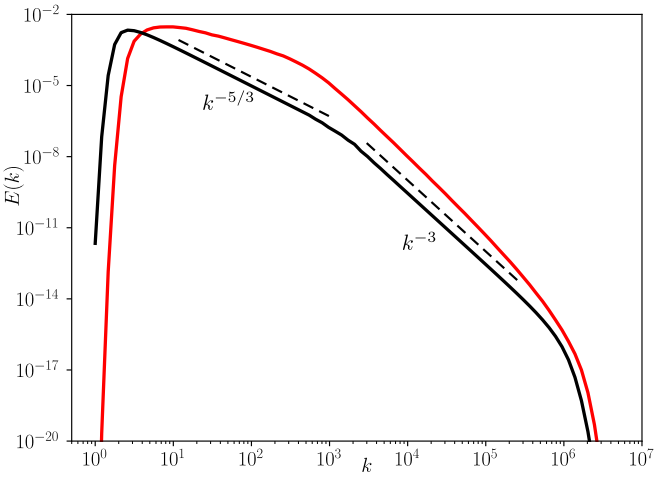

FIG. 4. Wave-number spectra for the two variants of the $\ell = 1$, $m = 3$ spiral chain model. The red line (if in color) is the model for the complex amplitude Φ_n, whereas the black line is the model for E_n. While the model for E_n is driven with constant forcing $P_n = 2.5 \times 10^{-4}$, the model for Φ_n is driven with random forcing such that $\langle P_n \rangle = 2.5 \times 10^{-4}$. The spectrum for the Φ_n model is averaged over a long stationary phase, where $E(k_n) = \langle |\Phi_n|^2 \rangle k_n$, which is integrated up to $t = 10\,000$ and the average is computed over $t = [5000, 10\,000]$, whereas the spectrum for the E_n model is averaged over $t = [190, 200]$ (in fact the instantaneous solution is not that different from the averaged result).

The spiral grid corresponding to the four-spiral chain, and its reflection with respect to the origin, is also shown in Fig. 3. The grid provides an alternative way of looking at the spiral chain as a partition of the k-space. The surface element for a given cell n can then be written as

$$S_n = \frac{\pi(g^1 - g^{-1})(g^5 - g^{-5})}{20 \ln(g)} k_n^2 \approx 0.03534 \times \pi k_n^2,$$

which is basically a small percentage of the area of the circle with that same radius. One obvious problem with this perspective is the "hole" that it leaves at the center. One can remedy this either by computing the actual shape of the leftover region and adding it as a partition cell, or alternatively by adding a circular cell around the origin and reducing the surface elements of the first few cells of the partition by subtracting the part of the circular region that intersects with the cell that is left for the circular element defined at the origin. While rather promising, spiral partitioning of k-space is not the focus of this paper. Thus we leave it for future studies to resolve its particular issues.

V. NUMERICAL RESULTS

Existence of all possible triads enabled by neatly matching grid points of a regular mesh allows important advantages such as good statistical behavior, mathematical clarity, and use of efficient numerical methods such as fast Fourier transforms. The models that we present in this paper are not likely to replace direct numerical simulation schemes such as pseudospectral methods even when very large wave-number ranges are needed. Instead, they may be used as models of cascade that can provide a mathematical framework for understanding the detailed structure of the cascade process through self-similar triad interactions.

Various models introduced in this paper can be considered as sets of ordinary differential equations that can be solved numerically in the presence of well-localized forcing and dissipation in the hope of establishing numerical inertial range cascade behavior. However, note that the primary goal of this paper is to introduce the framework of spiral chains and not to perform a detailed numerical study of these models.

The results for the basic chain model for complex amplitudes Φ_n's for the chain $\ell = 1$, $m = 3$, driven with stochastic forcing, with dissipation of the form $D_n = (\nu k^4 + \nu_L / k^6)\Phi_k$, can be seen in Figs. 4 and 5 along with the model for E_n for comparison. Even though the evolution of the complex phase is due to nonlinear couplings, the phases rapidly become "random" in practice, causing the fluxes to oscillate (both in time and along the chain), resulting in a statistical chain equipartition solution, which overwhelms the cascade process. In contrast the results for the chain model for E_n for $\ell = 1$, $m = 3$ show a clear dual cascade and thus a distinct Kraichnan-Kolmogorov spectrum. Here we used a simple Python solver [46], based on scipy ode solver [47].

The four-chain model introduced in Sec. IV B has a good coverage of the k-space both in radial and in angular directions. Here we present the 2D wave-number spectrum that we obtain from this model, with $N = 440$, $\nu = 10^{-24}$, $\nu_L = 10$, and anisotropic forcing $P_n^E = 2.5 \times 10^{-4}$ for the four wave numbers closest to $k_x = 0$, $k_y = \pm 2 \times 10^3$ in Fig. 6. Even though the drive is anisotropic, the resulting spectrum is isotropic since the flux along the spiral chain results naturally in isotropization of the spectrum. The time evolution of the wave-number spectrum is shown in Fig. 7, and the fluxes are shown in Fig. 8. Finally no intermittency has been observed in any of the models for E_n, since $S_j(k_n) \equiv \langle E_n^{j/2} \rangle \sim k_n^{-j/3}$ for

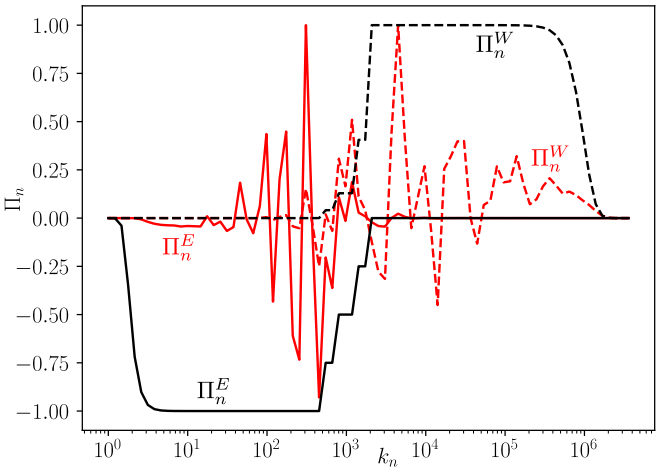

FIG. 5. Energy and enstrophy fluxes for the two variants of the $\ell = 1, m = 3$ spiral chain model. The red solid and dashed lines (if in color) are the energy and enstrophy fluxes for the complex amplitude model, whereas the black solid and dashed lines are the energy and enstrophy fluxes for the E_n model, respectively, normalized to their maximum values. We can see that rapid oscillations of the phases observed in the complex model cause the suppression of the fluxes and result in statistical chain equipartition solutions instead of proper dual cascade solutions.

the inverse cascade range and $S_j(k_n) \equiv \langle E_n^{j/2} \rangle \sim k_n^{-j}$ for the forward cascade range, with no discernible correction.

Physical real space fields such as the stream function and the vorticity can be obtained from the spiral chain

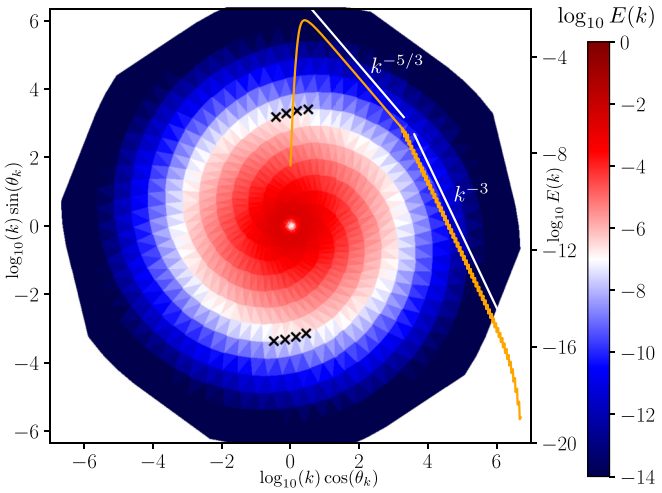

FIG. 6. Two-dimensional "log-log," i.e., $\{\log_{10}(k)\cos(\theta_k), \log_{10}(k)\sin(\theta_k), \log_{10}[E(k)]\}$, plot of the wave-number spectrum for the four-spiral chain model discussed in Sec. IV B. The energy injection is located around $k_x = 0$, $k_y = \pm 2 \times 10^3$, shown as black ×'s. The resulting spectrum consists of a clear inverse energy cascade range of $E(k) \propto k^{-5/3}$ (the red central region) and a forward enstrophy cascade range of $E(k) \propto k^{-3}$ (the blue peripheral region). A one-dimensional spectrum, which can be obtained by plotting $\mathrm{E}(k_n) = E_n/k_n$ as a function of $k_n = |\mathbf{k}_n|$, is also shown with guiding lines showing the theoretical predictions.

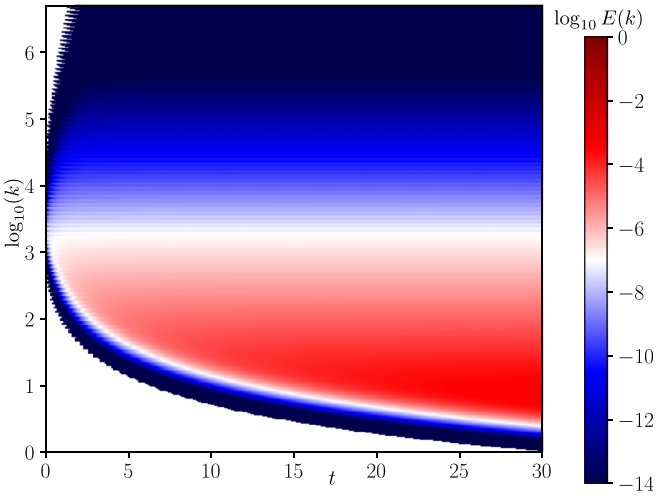

FIG. 7. Time evolution of the one-dimensional k-spectrum, showing how it gets established in time in an asymmetric nonlinear diffusion where the small scales are rapidly filled while large scales take a while to populate. Here the colors show different levels of $E(k)$, where as before the red region between $\log(k) = 0$ and 3 corresponds to the inverse cascade and the blue region between 4 and 6 corresponds to the forward cascade region as in Fig. 6.

representation of Φ_n as

$$\Phi(\mathbf{x}, t) = \sum_n \Phi_n(t) e^{i\mathbf{k}_n \cdot \mathbf{x}}, \quad \omega(\mathbf{x}, t) = \sum_n k_n^2 \Phi_n(t) e^{i\mathbf{k}_n \cdot \mathbf{x}}. \quad (23)$$

Since Φ_n does have the phase information, $\Phi(\mathbf{x}, t)$ does have detailed spatial structure and its evolution. However, for the model based on E_n, the phase information is lost, and if we use $\Phi_n = \sqrt{E_n} k_n^{-1}$ in (23), we get a fractal-like structure localized at the origin (see Fig. 9). The physical structure of the fractal consists of discrete logarithmic spirals, where each point of the spiral is another spiral centered around that point. The weights are such that in the end we get a $k^{-5/3}$ spectrum for

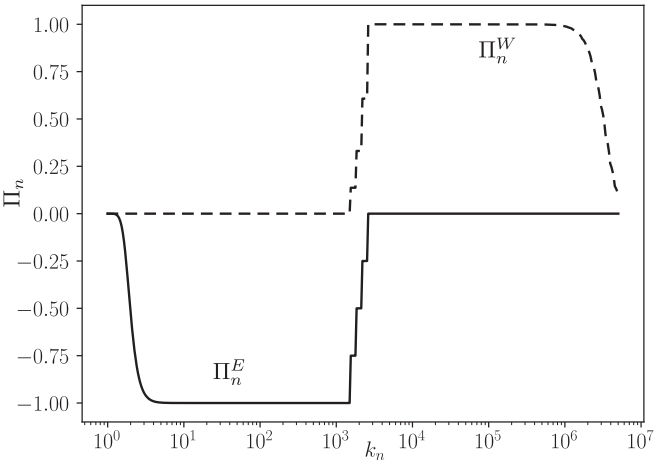

FIG. 8. Energy and enstrophy fluxes Π_n^E and Π_n^W, normalized to their maximum values, for the four-spiral chain model. This is averaged over 10 time steps, but even instantaneously, they are extremely flat and stationary.

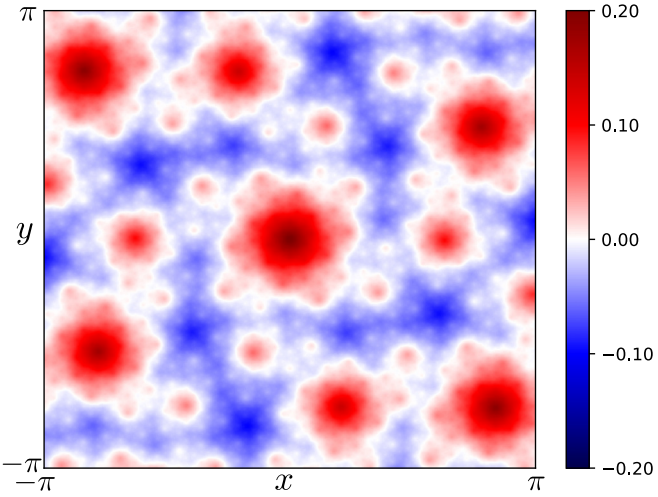

FIG. 9. Snapshot of the stream function $\Phi(\mathbf{x}, t)$ obtained from the spiral chain model with $\ell = 1$, $m = 3$ for the evolution of E_n. The fractal structure that we observe consist of discrete logarithmic spirals, where each point of the spiral is a spiral in itself centered around that point. The weights are such that in the end we obtain a $k^{-5/3}$ spectrum for energy.

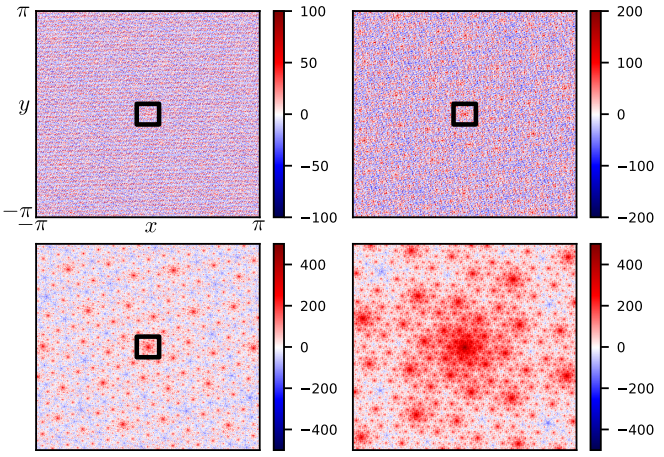

FIG. 10. Snapshot of the vorticity field $\omega(\mathbf{x}, t)$ obtained from the spiral chain model with $\ell = 1$, $m = 3$ for the evolution of E_n. Low-pass filtered vorticity field is shown at the top left plot. The box in the center (which is 1/10 of the original box) is then expanded to show the band-passed filtered vorticity field on the top right. The box in the center of this plot is then expanded to show the band-pass filtered vorticity field on the bottom left and so on. The fractal structure, which consists of discrete logarithmic spirals, where each point of the spiral is a spiral centered around that point, is now visible mainly at the smallest spatial scales (lower right plot). This is actually the other end of the same fractal structure visible for the large scales in Fig. 9 for the stream function. The weights of the fractal form at those smaller scales are such that we have a k^{-3} spectrum for energy.

$E(k)$, since what we see in Fig. 9 is mainly the inverse cascade range (i.e., because the spiral chain has extremely high effective resolution, when we switch to spatial representation with a finite resolution, we are effectively using a low-pass filtered version of the field). Similarly for the vorticity field, we see basically white noise at large scales and the *hierarchical spiral fractal* structure with k^{-3} scaling for the $E(k)$ for the small scales as seen in Fig. 10. The fractal structure grows from an initial crystal-like state that corresponds to the drive, and once the growth is completed, the E_n model remains stationary.

VI. CONCLUSION

The geometry of the self-similar dual cascade in two dimensions as the energy or enstrophy is transferred from one wave vector to another through triadic interactions is considered. The resulting picture is that of a chain of triangles that are rotated and scaled, such that the smallest wave number of one triangle becomes the middle and largest wave numbers of the consecutive triads. A particular class of triangles make it such that one can form regular logarithmic spiral grids out of the wave numbers $\mathbf{k}_n = k_0(ge^{i\alpha})^n$, where the complex number is interpreted as a 2D vector so that the real and imaginary parts are the x and y components, with g and α being the scaling factor and the divergence angle, respectively. Nonlinear interactions take place among the wave vectors $\mathbf{k}_n$, $\mathbf{k}_{n+\ell}$, and $\mathbf{k}_{n+m}$ on such a spiral, where the values of ℓ and m define (not necessarily uniquely) particular values of g and α. There is, in fact, a large number of such triangles, some of which are listed explicitly in Table I. It is argued that the self-similar cascade takes place along triad chains, and therefore the concept of spiral chains can give us better insight into this mechanism, without the explicit assumption of isotropy.

In order to demonstrate the usefulness of the concept, a series of spiral chain models both for the complex amplitudes Φ_n as well as for energy E_n have been developed. It is shown that analytical solutions of these models agree with the Kraichnan-Kolmogorov phenomenology of isotropic cascade. The complex models, however, which are basically "shell models" with elongated triads, cannot numerically reproduce the dual cascade (because the nonlinear evolution of the phases leads to oscillatory solutions for the fluxes of conserved quantities) and instead converge to unphysical chain equipartition solutions. The model for E_n in (19) can reproduce the dual cascade results numerically for any ℓ and m.

In particular, a four-spiral chain model for E_n is introduced in (22), which has good angular coverage and has two kinds of triads because of the choice of g and α to include $\ell = 2$, $m = 3$ and $\ell = 1$, $m = 5$ simultaneously. While a simple test of anisotropic energy injection leads to the usual isotropic dual cascade result, the model can be developed for a self-consistent drive or other similar cases for more complex problems such as 2D plasmas or geophysical fluids.

ACKNOWLEDGMENT

The authors would like to thank P. H. Diamond, W.-C. Müller, and attendees of the Festival de Théorie, Aix en Provence, in 2017.

[1] G. Boffetta and R. E. Ecke, Annu. Rev. Fluid Mech. **44**, 427 (2012).
[2] R. H. Kraichnan and D. Montgomery, Rep. Prog. Phys. **43**, 547 (1980).
[3] R. H. Kraichnan, Phys. Fluids **10**, 1417 (1967).
[4] G. Boffetta and S. Musacchio, Phys. Rev. E **82**, 016307 (2010).
[5] G. K. Vallis, *Atmospheric and Oceanic Fluid Dynamics: Fundamentals and Large-Scale Circulation* (Cambridge University Press, Cambridge, 2006).
[6] F. Bouchet and A. Venaille, Phys. Rep. **515**, 227 (2012).
[7] W. Horton and A. Hasegawa, Chaos **4**, 227 (1994).
[8] P. H. Diamond, A. Hasegawa, and K. Mima, Plasma Phys. Control. Fusion **53**, 124001 (2011).
[9] G. Depret, X. Garbet, P. Bertrand, and A. Ghizzo, Plasma Phys. Control. Fusion **42**, 949 (2000).
[10] T. Drouot, E. Gravier, T. Reveille, A. Ghizzo, P. Bertrand, X. Garbet, Y. Sarazin, and T. Cartier-Michaud, Eur. Phys. J. D **68**, 280 (2014).
[11] S. Xu, P. Morel, and Ö. D. Gürcan, Phys. Plasmas **25**, 022304 (2018).
[12] S. Xu, P. Morel, and Ö. D. Gürcan, Phys. Plasmas **25**, 102306 (2018).
[13] M. McIntyre and W. Norton, J. Atmos. Sci. **57**, 1214 (2000).
[14] C. J. McDevitt, P. H. Diamond, O. D. Gürcan, and T. S. Hahm, Phys. Plasmas **17**, 112509 (2010).
[15] Ö. D. Gürcan and P. H. Diamond, J. Phys. A **48**, 293001 (2015).
[16] L. Biferale, Annu. Rev. Fluid Mech. **35**, 441 (2003).
[17] I. Adler, D. Barabe, and R. V. Jean, Ann. Botany **80**, 231 (1997).
[18] S. Douady and Y. Couder, J. Theor. Biol. **178**, 255 (1996).
[19] A. C. Newell, P. D. Shipman, and Z. Sun, J. Theor. Biol. **251**, 421 (2008).
[20] E. J. Crampin, W. W. Hackborn, and P. K. Maini, Bull. Math. Biol. **64**, 747 (2002).
[21] T. S. Lundgren, Phys. Fluids **25**, 2193 (1982).
[22] A. D. Gilbert, J. Fluid Mech. **193**, 475 (1988).
[23] U. Frisch, *Turbulence: The Legacy of A. N. Kolmogorov* (Cambridge University Press, Cambridge, 1995).
[24] A. Alexakis and L. Biferale, Phys. Rep. **767–769**, 1 (2018).
[25] K. Ohkitani and M. Yamada, Prog. Theor. Phys. **81**, 329 (1989).
[26] C. E. Leith, Phys. Fluids **10**, 1409 (1967).
[27] D. K. Lilly, J. Atmos. Sci. **46**, 2026 (1989).
[28] V. S. L'vov and S. Nazarenko, JETP Lett. **83**, 541 (2006).
[29] R. H. Kraichnan, J. Fluid Mech. **5**, 497 (1959).
[30] S. A. Orszag, J. Fluid Mech. **41**, 363 (1970).
[31] E. Aurell, P. Frick, and V. Shaidurov, Physica D **72**, 95 (1994).
[32] E. Aurell, E. Dormy, and P. Frick, Phys. Rev. E **56**, 1692 (1997).
[33] F. Waleffe, Proc. Am. Math. Soc. **134**, 2913 (2006).
[34] S. Grossmann, D. Lohse, and A. Reeh, Phys. Rev. Lett. **77**, 5369 (1996).
[35] S. S. Ray, Pramana **84**, 395 (2015).
[36] S. S. Ray, U. Frisch, S. Nazarenko, and T. Matsumoto, Phys. Rev. E **84**, 016301 (2011).
[37] E. Aurell, G. Boffetta, A. Crisanti, P. Frick, G. Paladin, and A. Vulpiani, Phys. Rev. E **50**, 4705 (1994).
[38] J. Pedlosky, *Geophysical Fluid Dynamics*, 2nd ed. (Springer-Verlag, New York, 1987).
[39] F. S. Godeferd and F. Moisy, Appl. Mech. Rev. **67**, 030802 (2015).
[40] P. B. Rhines, Annu. Rev. Fluid Mech. **11**, 401 (1979).
[41] W. Horton, Rev. Mod. Phys. **71**, 735 (1999).
[42] M. De Pietro, L. Biferale, and A. A. Mailybaev, Phys. Rev. E **92**, 043021 (2015).
[43] V. S. L'vov, A. Pomyalov, and I. Procaccia, Phys. Rev. Lett. **89**, 064501 (2002).
[44] U. Frisch, A. Pomyalov, I. Procaccia, and S. S. Ray, Phys. Rev. Lett. **108**, 074501 (2012).
[45] A. Monin and A. Yaglom, in *Statistical Fluid Mechanics: Mechanics of Turbulence*, edited by J. Lumley, Vol. 2 (MIT Press, Cambridge, MA, 1975).
[46] Ö. D. Gürcan, Spiral chain models, https://github.com/gurcani/scms (2019).
[47] E. Jones, T. Oliphant, P. Peterson, *et al.*, SciPy: Open source scientific tools for Python (2001), http://www.scipy.org/.